Infrared flash kinetic spectroscopy of HCO

C. Brent Dane, D. R. Lander, R. F. Curl, and F. K. Tittel
Chemistry and Electrical Engineering Departments and Rice Quantum Institute, Rice University, Houston, Texas 77251

Yili Guo, Martin I. F. Ochsner,[a] and C. Bradley Moore
Materials and Molecular Research Division, Lawrence Berkeley Laboratory and Department of Chemistry, University of California, Berkeley, California 94720

(Received 7 October 1987; accepted 27 October 1987)

The high resolution infrared spectrum of the CH stretching fundamental of the formyl radical (HCO) has been observed by means of infrared kinetic spectroscopy using 308 nm (XeCl) excimer laser flash photolysis of formaldehyde or acetaldehyde followed by diode or difference frequency laser probing of the transient absorption. The high resolution spectra obtained were assigned and fitted with rotational, spin–rotational, and centrifugal distortion constants. The ν_1 band origin is 2434.48 cm^{-1}. New ground-state constants are reported from a least-squares fit combining this ν_1 data with previous microwave and FIR LMR measurements.

INTRODUCTION

Formyl radical is an important intermediate in combustion and atmospheric chemistry. It is particularly interesting structurally and chemically because of its unusually weak and anharmonic CH bond. Consequently it has been the subject of numerous spectroscopic investigations.[1] With regard to high resolution studies of the vibrational spectrum, the bending fundamental (1080.76 cm^{-1}) has been observed by LMR[2] and laser stark spectroscopy[3] and the CO stretching fundamental (1868.17 cm^{-1}) has been observed by LMR.[4,5] The CH stretching fundamental has not previously been measured in the gas phase although the CD stretch of DCO (1909.77 cm^{-1}) has been observed by LMR.[6] All of the above studies probe only small portions of a vibration–rotation band near a fixed-frequency laser source. The data consequently contain little information on the energy differences between levels with different K_a quantum numbers. Broadly tunable IR lasers are used in this work to record a large part of the CH stretching vibration–rotation band at high resolution. The analysis completes the high resolution determination of the fundamental vibrational frequencies of HCO and provides improved constants for rotation about the a axis.

EXPERIMENTAL

Difference frequency laser spectra

The difference frequency laser kinetic spectroscopy apparatus (Berkeley) had been described previously.[7] A tunable difference frequency laser system, similar to the one developed by Pine,[8] provides tunable CW infrared light near 4.2 μm having a linewidth of $\sim$0.0007 cm^{-1}. The output of a single mode, CW Ar^+ laser (Lexel 95-4, 1 W at 514.5 nm) is combined with an Ar^+-pumped, tunable, single mode, CW ring dye laser (Spectra-Physics 171-06/380) and focused onto a temperature-phase-matched $LiNbO_3$ crystal. The photolysis laser is a Lambda Physik EMG 103E operated on the XeCl (308 nm) line at 60 Hz with a pulse energy of 30–40 mJ.

The infrared probe and photolysis laser propagate collinearly through the photolysis cell and are then separated after emerging by a UV-reflecting IR-transmitting sapphire mirror. A narrow-band IR filter is used to eliminate broadband IR fluorescence from the excimer discharge. The IR probe is detected by an InSb (77 K) detector. The resulting signal is amplified by two low-noise amplification stages and integrated by a dual channel boxcar integrator (PAR 162/164) with a 60 μs gate and 50 μs input time constant. The signal gate (of the boxcar) opens 1 μs after the reference gate closes. The excimer laser fires during the 1 μs time interval. A microcomputer A/D reads the difference between the two boxcar signals after each photolysis pulse and averages it over 25 shots for each frequency increment.

Overlapping scans of 3 cm^{-1} were recorded to give a continuous spectrum of 200 cm^{-1} including some 750 observed absorption lines. The HCO line positions were determined by measuring simultaneously the fluorescence excitation spectrum of iodine vapor and using the tabulated frequencies.[9] The instability of the Ar^+ laser limits the accuracy to $\pm$ 0.01 cm^{-1}.

Both formaldehyde and acetaldehyde (2.5 Torr of pure gas flowing at 100 l/min) were used as HCO precursors. Similar S/N and identical line positions were obtained for each. A few wave numbers of the HCO spectrum were blocked by acetaldehyde absorption but observed with formaldehyde. Formaldehyde was prepared as previously described[10] and acetaldehyde (Mallinckrodt) was purified by vacuum distillation.

Diode laser spectra

The diode laser kinetic spectroscopy apparatus (Rice University) is shown in Fig. 1. In brief, transient infrared absorption of the diode laser beam by HCO produced by XeCl (308 nm) flash photolysis of acetaldehyde is detected by acquiring the output of the signal detector with a transient digitizer (Biomation 805) immediately before and after the excimer laser flash. The diode laser system and its method of operation for normal absorption spectroscopy has been described previously.[11] Data acquisition from the transient digitizer was added in a straightforward manner. Tran-

[a] Present address: CIBA-GEIGY A.G., Analytische Forschung FO3.2 CH-4002, Basel Switzerland.

 0021-9606/88/042121-08$02.10

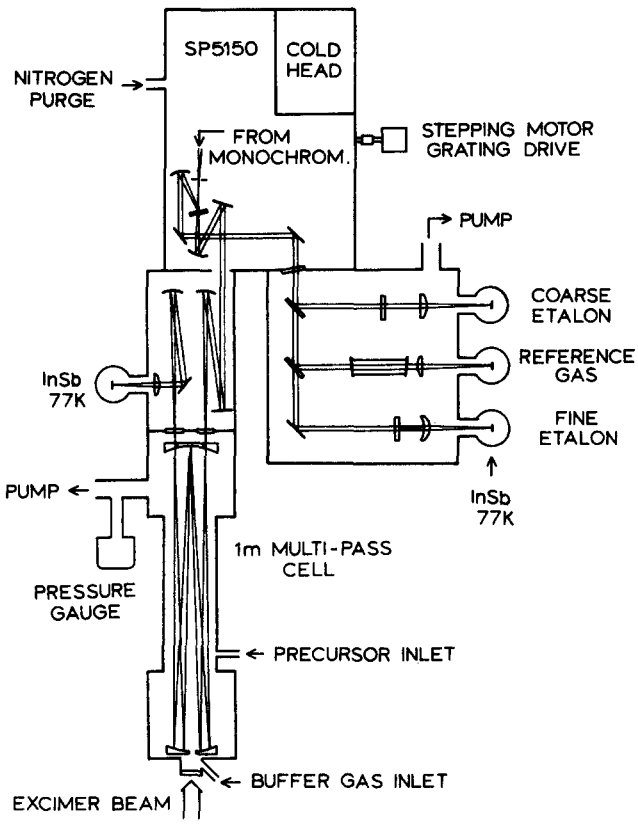

FIG. 1. Schematic of the diode laser flash kinetic infrared spectrometer. The White cell was operated with a 52 m pathlength although the actual overlap between the UV photolysis beam and the infrared probe is significantly less.

sient absorption spectroscopy is carried out in a multiple reflection cell. In order to obtain maximum overlap between the infrared probe beams and the region photolyzed, the excimer laser beam is introduced just below the *D* mirrors of the White cell and intercepted by a beam block just in front of and above the upper row of probe infrared beam spots on the notched mirror. By flowing helium continuously into and through the *D* mirror chamber and introducing the precursor acetaldehyde flow downstream about 25 cm into the cell, "dead space" absorption of the excimer beam by the precursor is minimized. Since the excimer beam and its accompanying infrared fluorescence never actually strike the White cell mirrors, infrared interference from the excimer is small. Typical operating conditions were total pressure = 7.5 Torr, acetaldehyde pressure = 2.5 Torr, acetaldehyde flow rate = 60 scc/min, excimer repetition rate = 20 Hz, and excimer pulse energy = 75 mJ.

HCO frequencies were measured by acquiring a reference calibration spectrum of N_2O simultaneously during each scan and interpolating tabulated[12] N_2O line positions with an accurately calibrated 500 MHz vacuum spaced marker cavity. Generally the accuracy of the resulting line positions is limited by the accuracy of the calibration lines which is typically ± 0.001 cm^{-1}.

RESULTS

Observations and assignment

The region to be searched for the HCO CH stretch was estimated using the matrix isolation CH stretching frequency[13] of 2483 cm^{-1} and the CH stretching frequency estimated from laser fluorescence[14] of 2432 $\pm$ 20 cm^{-1}. A number of lines of a transient species produced by the flash photolysis of formaldehyde were first observed by the difference frequency system with a S/N of 12 for the strongest lines using a single boxcar, and were postulated to be *R*-branch lines of the CH stretch of HCO. The strongest transitions corresponded to about 10% attenuation of the IR power. Unfortunately the low frequency tuning limit of the difference frequency system did not allow observation of *a*-type *Q* branches, which complicated the assignment of the observed spectrum.

The diode laser used in this study overlaps somewhat the low frequency end of the difference frequency scans and continues to operate well through the band origin region. Very good sensitivity for HCO could be obtained with the diode laser kinetic spectroscopy by averaging transient digitizer points for 25 μs before and after the flash and differencing. Using acetaldehyde as the precursor, S/N ratios of $\sim$200 could be obtained for the strongest lines corresponding to a $\sim$15% absorption of the infrared probe. Figure 2 depicts the $K = 3$ *a*-type *Q*-branch region obtained with the diode system.

The rotational assignment of this spectrum proved to be straightforward. Two obvious parallel *Q* branches were found in the diode laser scans. The relative intensity of the

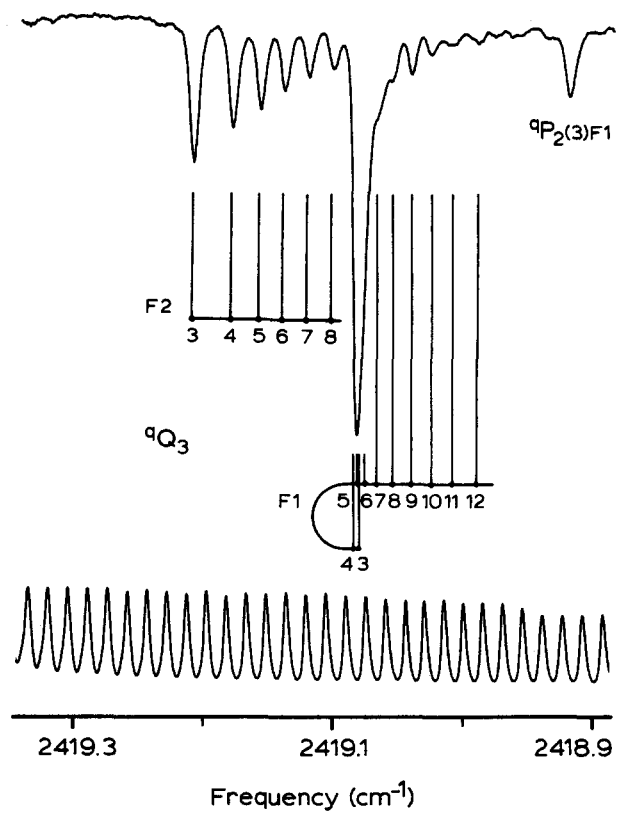

FIG. 2. $K = 3$ parallel *Q* branches of the CH stretching fundamental of HCO. 50 transient digitizer points each of 500 ns duration are averaged immediately before and after each excimer shot and subtracted. The laser is stepped 20 MHz in scanning with 30 shots averaged per step. The asymmetry splittings are not resolved. Conditions: He pressure = 5 Torr, acetaldehyde pressure = 2.5 Torr, XeCl pulse energy = 75 mJ, repetition rate = 20 Hz. Pictured as well are the 500 MHz étalon fringes used in laser scanning and calibration.

second to the first member of each suggested that the high frequency Q branch belonged to $K = 3$ and the lower frequency one to $K = 4$. Using the previously measured ground-state rotational, spin–rotational, and centrifugal distortion constants,[15,16] P- and R-branch lines could be predicted and were identified confirming the $K = 3$ and 4 parallel Q-branch assignments. The information thus obtained located the approximate positions of the $K = 1$, 2, and 5 Q branches. Several lines of the $K = 1$ Q-branch series and the characteristic four line patterns of the corresponding P and R branches were quickly recognized. By fitting on these lines, many additional lines were predicted and assigned in the diode and difference frequency data. Figure 3 shows the $K = 3 \leftarrow 2$ Q-branch region observed with the difference frequency laser system. The S/N of the difference frequency system is improved by a factor of about 10 with the dual gated integrator arrangement used for recording the spectra reported here. Table I lists 100 of the 780 (610 difference frequency, 170 diode) parallel- and perpendicular-type rotational transitions assigned using the two spectrometers. A complete listing of all the observed transition frequencies will be given in the Ph.D. theses of Guo (Berkeley) and Dane (Rice).

HCO is relatively long-lived in this system as can be seen by the transient digitizer trace of its decay shown in Fig. 4. The principal loss mechanism for HCO is probably the disproportion of two HCO molecules to produce CO and H_2CO as evidenced by the roughly second-order decay curve. Diffusion out of the probe beam is another possible source of signal loss, but is minimized in this system by the 10 cm diameter of the White cell and the fact that the excimer beam passes down the center of the cell. Preliminary measurements of HCO decay rates in the presence of varying pressures of O_2 have been made and the resulting rate constant for the reaction $HCO + O_2 \rightarrow CO + H_2O$ is equal to the published measurement[17] within experimental uncertainty.

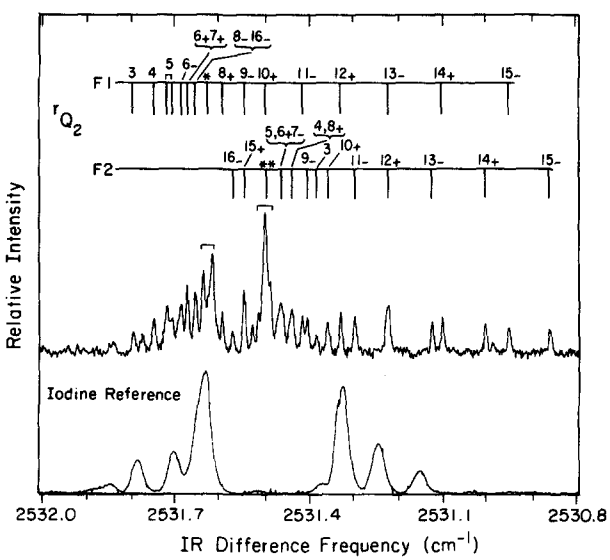

FIG. 3. $K = 3 \leftarrow 2$ perpendicular Q branches. 25 shots are averaged for each frequency step (0.0015 cm^{-1}). The IR spectrum linewidths ($\sim$0.01 cm^{-1}) are Doppler limited. The subscript + or − in the assignment stands for even or odd K_c'' parity, respectively. Subscripts are omitted when asymmetry splittings are not resolved. *Overlapped transitions of 9 +, 7 −, 15 +, 10 −, 14 −, 11 +, 12 −, 13 +. **Overlapped transitions of 14 −, 13 +, 12 −, 11 +, 10 −, 9 +, 8 −, 7 +. Conditions: Acetaldehyde pressure = 2.5 Torr, XeCl pulse energy = 35 mJ, repetition rate = 60 Hz.

Least-squares fit

Initially the observed transitions were least-squares fitted with a band origin and upper state rotational, spin–rotational, and centrifugal distortion constants using Watson's A-reduced Hamiltonian[18] and the spin–rotation formulation of Brown and Sears.[19] The fitting program was checked by comparing predictions and least-square fitting against output of the program of Sears[20] and good agreement was found. When such a fitting was carried out, it was found that the $K' = 4$ and $K' = 5$ infrared transitions appeared to be incompatible with each other. When transitions involving levels from both stacks were included, the standard deviation became about 2.5 times that expected from the estimated errors in the measurements, almost tripling in comparison with the standard deviation obtained when only either $K' = 4$ or $K' = 5$ transitions were included in the fit. This could not be remedied by including additional centrifugal distortion constants of higher order in K even though $K' = 5$ is the highest K' assigned. It seems that the apparent perturbation in the upper state can be ascribed primarily to the $K' = 4$ levels, since if these lines are included there are systematic deviations in the $K' = 3$ levels and several of the upper state centrifugal distortion and spin–rotational centrifugal distortion constants change by what seem to be unreasonably large amounts from the ground state. However, as discussed later, there are still significant changes in Δ_{NK} and Φ_{KN} even when the $K' = 4$ lines are omitted.

It is suspected that the $K' = 4$ transitions may be affected by Coriolis interaction with the $K' = 5$ levels of the bending overtone. The A rotational constant of the bending overtone is expected to be much larger than the A value of this CH stretch excited state, so that even though the bending overtone is near 2000 cm^{-1} the energies of a level of given K will catch up with the $K - 1$ and eventually with the K levels of the 2400 cm^{-1} CH stretch as K increases. Figure 5 depicts an estimate of the relative locations of the (1,0,0) and (0,0,2) K stacks based upon the relative location of the two vibrational levels obtained from the HCO-photoelectron spectrum[21] and upon the bending vibration–rotation interaction constants.[2] The $K' = 4$ levels appear to be pushed down by increasing amounts with increasing N' with a maximum displacement of about 0.2 cm^{-1} near the largest observed N' of 23 as seen in the residuals from the least-squares fit presented in Fig. 6. Such a displacement could result from a Coriolis interaction between $(0,0,2)K = 5$ and $(1,0,0)K = 4$. The slow onset is readily explained by the fact that $(B + C)/2$ for (1,0,0) is, in fact, expected to be slightly smaller than $(B + C)/2$ for (0,0,2). Thus by $N = 20$ the separation between the two levels is expected to *increase* by almost 0.5 cm^{-1} from its smallest value at $N = 5$. Thus it is believed that the increasing size of the perturbation with N results because the Coriolis matrix element[22] is proportional to $[N(N + 1) - 20]^{1/2}$ and the energy difference between the two interacting levels is almost independent of N.

Having recognized that some of the upper state levels

TABLE I. A selection of 100 of the 780 infrared transitions of HCO measured and assigned in this study.

ν(cm^{-1})[a]	N_{KaKc}	J	Obs. − calc. (10^{-3}cm^{-1})	ν(cm^{-1})[b]	N_{KaKc}	J	Obs. − calc. (10^{-3}cm^{-1})
2263.989	$14_{3,12} \leftarrow 14_{4,11}$	13.5 ← 13.5	1	2447.941	$10_{38} \leftarrow 9_{37}$	10.5 ← 9.5	5
2264.013	$13_{3,10} \leftarrow 13_{49}$	12.5 ← 12.5	−1	2448.018	$10_{38} \leftarrow 9_{37}$	9.5 ← 8.5	11
2264.081	$10_3 \leftarrow 10_4$	9.5 ← 9.5	1	2452.512	$7_{17} \leftarrow 6_{16}$	7.5 ← 6.5	15
2264.109	$9_3 \leftarrow 9_4$	8.5 ← 8.5	1	2452.524	$7_{17} \leftarrow 6_{16}$	6.5 ← 5.5	10
2264.138	$8_3 \leftarrow 8_4$	7.5 ← 7.5	−1	2453.319	$7_{16} \leftarrow 6_{15}$	7.5 ← 6.5	−1
2264.175	$7_3 \leftarrow 7_4$	6.5 ← 6.5	−1	2453.335	$7_{16} \leftarrow 6_{15}$	6.5 ← 5.5	0
2264.221	$6_3 \leftarrow 6_4$	5.5 ← 5.5	0	2455.600	$14_{0,14} \leftarrow 13_{1,13}$	c	10
2264.283	$5_3 \leftarrow 5_4$	4.5 ← 4.5	1	2549.217	$9_{18} \leftarrow 8_{17}$	8.5 ← 7.5	9
2264.378	$4_3 \leftarrow 4_4$	3.5 ← 3.5	2	2464.913	$13_{2,12} \leftarrow 12_{2,11}$	13.5 ← 12.5	−5
2393.650	$10_5 \leftarrow 10_5$	9.5 ← 9.5	−1	2464.937	$13_{2,12} \leftarrow 12_{2,11}$	12.5 ← 11.5	−4
2393.676	$9_5 \leftarrow 9_5$	8.5 ← 8.5	0	2470.928	$13_{1,12} \leftarrow 12_{1,11}$	c	−3
2393.700	$8_5 \leftarrow 8_5$	7.5 ← 7.5	0	2473.434	$16_{2,15} \leftarrow 15_{2,14}$	16.5 ← 15.5	−7
2393.726	$7_5 \leftarrow 7_5$	6.5 ← 6.5	1	2473.448	$16_{2,15} \leftarrow 15_{2,14}$	15.5 ← 14.5	−10
2393.753	$6_5 \leftarrow 6_5$	5.5 ← 5.5	1	2473.817	$16_{2,14} \leftarrow 15_{2,13}$	16.5 ← 15.5	−6
2393.785	$5_5 \leftarrow 5_5$	4.5 ← 4.5	−1	2473.832	$16_{2,14} \leftarrow 15_{2,13}$	15.5 ← 14.5	−6
2407.796	$4_4 \leftarrow 4_4$	3.5 ← 3.5	−8[d]	2481.673	$10_{1,10} \leftarrow 9_{09}$	9.5 ← 8.5	0
2410.531	$6_{06} \leftarrow 6_{15}$	6.5 ← 6.5	−2	2481.682	$10_{1,10} \leftarrow 9_{09}$	10.5 ← 9.5	−2
2410.601	$6_{06} \leftarrow 6_{15}$	5.5 ← 5.5	0	2492.260	$12_{2,10} \leftarrow 12_{1,11}$	11.5 ← 11.5	2
2414.200	$6_{06} \leftarrow 7_{07}$	c	1	2492.315	$12_{2,10} \leftarrow 12_{1,11}$	12.5 ← 12.5	3
2415.118	$5_{14} \leftarrow 6_{15}$	c	1	2496.641	$6_{25} \leftarrow 6_{16}$	5.5 ← 5.5	3
2417.098	$5_{05} \leftarrow 6_{06}$	c	−2	2496.790	$6_{25} \leftarrow 6_{16}$	6.5 ← 6.5	−1
2419.114	$8_3 \leftarrow 8_3$	7.5 ← 7.5	0	2499.250	$12_{2,11} \leftarrow 12_{1,12}$	11.5 ← 11.5	2
2419.133	$7_3 \leftarrow 7_3$	6.5 ← 6.5	−1	2499.346	$12_{2,11} \leftarrow 12_{1,12}$	12.5 ← 12.5	1
2419.151	$6_3 \leftarrow 6_3$	5.5 ← 5.5	−1	2509.553	$23_{1,23} \leftarrow 22_{0,22}$	23.5 ← 22.5	10
2419.169	$5_3 \leftarrow 5_3$	4.5 ← 4.5	−2	2509.662	$5_{24} \leftarrow 4_{13}$	4.5 ← 3.5	11
2419.191	$4_3 \leftarrow 4_3$	3.5 ← 3.5	−2	2509.797	$5_{24} \leftarrow 4_{13}$	5.5 ← 4.5	7
2419.221	$3_3 \leftarrow 3_3$	2.5 ← 2.5	−2	2510.605	$5_{23} \leftarrow 4_{14}$	4.5 ← 3.5	5
2420.980	$3_{12} \leftarrow 4_{13}$	2.5 ← 3.5	1	2510.758	$5_{23} \leftarrow 4_{14}$	5.5 ← 4.5	2
2420.991	$3_{12} \leftarrow 4_{13}$	3.5 ← 4.5	0	2519.671	$30_{1,29} \leftarrow 29_{1,29}$	29.5 ← 28.5	2
2421.074	$10_{1,10} \leftarrow 11_{0,11}$	9.5 ← 10.5	1	2519.955	$9_{28} \leftarrow 8_{17}$	8.5 ← 7.5	4
2421.090	$10_{1,10} \leftarrow 11_{0,11}$	10.5 ← 11.5	−1	2520.028	$9_{28} \leftarrow 8_{17}$	9.5 ← 8.5	4
2421.321	$3_{13} \leftarrow 4_{14}$	2.5 ← 3.5	1	2523.452	$9_{27} \leftarrow 8_{18}$	8.5 ← 7.5	−3
2421.337	$3_{13} \leftarrow 4_{14}$	3.5 ← 4.5	−1	2523.572	$9_{27} \leftarrow 8_{18}$	9.5 ← 8.5	11
2423.904	$2_{11} \leftarrow 3_{12}$	1.5 ← 2.5	1	2530.989	$14_{3,11} \leftarrow 14_{2,12}$	13.5 ← 13.5	−7
2423.932	$2_{11} \leftarrow 3_{12}$	2.5 ← 3.5	0	2531.085	$14_{3,11} \leftarrow 14_{2,12}$	14.5 ← 14.5	−2
2427.548	$2_2 \leftarrow 2_2$	4.5 ← 3.5	1	2545.960	$5_3 \leftarrow 4_2$	4.5 ← 3.5	4
2427.630	$2_2 \leftarrow 2_2$	2.5 ← 2.5	2	2546.136	$5_3 \leftarrow 4_2$	5.5 ← 4.5	−8
2430.579	$4_3 \leftarrow 3_3$	1.5 ← 1.5	−1	2557.450	$9_{37} \leftarrow 8_{26}$	8.5 ← 7.5	0
2430.916	$4_3 \leftarrow 3_3$	3.5 ← 2.5	−1	2557.511	$9_{36} \leftarrow 8_{27}$	8.5 ← 7.5	0
2432.627	$1_{11} \leftarrow 1_{10}$	1.5 ← 1.5	−1	2557.572	$9_{37} \leftarrow 8_{26}$	9.5 ← 8.5	0
2432.671	$1_{11} \leftarrow 1_{10}$	0.5 ← 0.5	0	2557.633	$9_{36} \leftarrow 8_{27}$	9.5 ← 8.5	−1
2432.826	$1_{10} \leftarrow 1_{11}$	1.5 ← 1.5	−1	2562.418	$17_{4,13} \leftarrow 17_{3,14}$	17.5 ← 17.5	−111[d]
2432.858	$1_{10} \leftarrow 1_{11}$	0.5 ← 0.5	0	2574.335	$4_{40} \leftarrow 3_{31}$	3.5 ← 2.5	−10[d]
2437.367	$1_{01} \leftarrow 0_{00}$	1.5 ← 0.5	0	2589.551	$8_5 \leftarrow 8_4$	8.5 ← 8.5	3
2441.222	$3_{13} \leftarrow 2_{12}$	3.5 ← 2.5	0	2589.582	$7_5 \leftarrow 7_4$	7.5 ← 7.5	0
2441.286	$3_{13} \leftarrow 2_{12}$	2.5 ← 1.5	−1	2589.617	$6_5 \leftarrow 6_4$	6.5 ← 6.5	−1
2445.111	$13_{4,10} \leftarrow 12_{49}$	12.5 ← 11.5	−65[d]	2606.767	$6_5 \leftarrow 5_4$	5.5 ← 4.5	−8
2445.648	$11_{0,11} \leftarrow 10_{1,10}$	11.5 ← 10.5	2	2606.897	$6_5 \leftarrow 5_4$	6.5 ← 5.5	2
2445.665	$11_{0,11} \leftarrow 10_{1,10}$	10.5 ← 9.5	0	2626.809	$13_5 \leftarrow 12_4$	12.5 ← 11.5	−9
2446.020	$4_{04} \leftarrow 3_{03}$	c	−1	2626.913	$13_5 \leftarrow 12_4$	13.5 ← 12.5	−5

[a] Diode laser measurements.
[b] Difference frequency laser measurements.
[c] Unresolved spin–splitting components.
[d] Transitions involving $K'_a = 4$ rotational levels were excluded from the excited state fit.

are possibly perturbed, it seemed appropriate to fit the ground state and excited state separately. The first step was to fit the ground state and thereby improve the ground state constants. Therefore, a least-squares fit of only the ground-state parameters was peformed combining the microwave transitions of Blake *et al.*,[15] the FIR LMR data,[16] and the ν_1 infrared data.

Rather than fitting combination differences which introduces the familiar problem[23] of observational correlation, we utilized a method in which an additional parameter was introduced for each upper state level to take into account the inadequacy of the upper state Hamiltonian. This appears to lead to a very large number of parameters to be determined and thus to a very large least-squares matrix to be inverted. However, the ground-state constants (rotational, centrifugal distortion, and spin–rotational) may be decoupled[24]

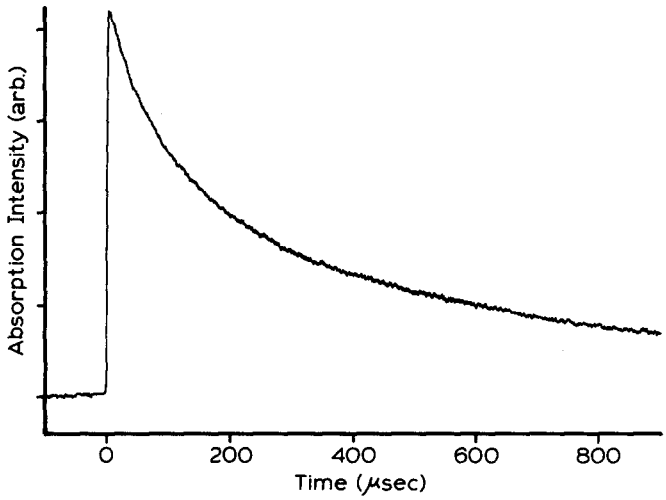

FIG. 4. Time decay of the signal from the $R_0(3)$ transition of HCO. The gas mixture conditions are the same as those of Fig. 2. 3000 traces are averaged.

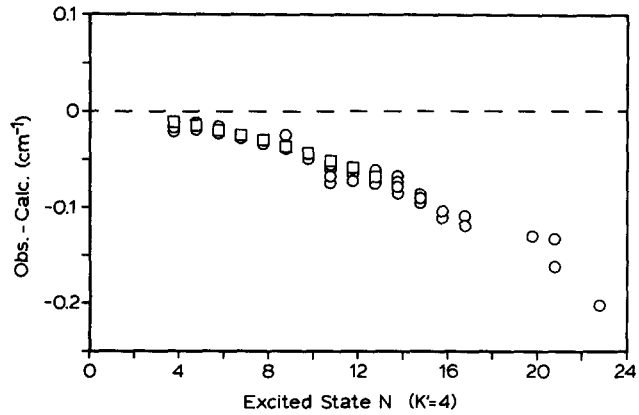

FIG. 6. Residuals of the observed transitions involving the $K' = 4$ rotational levels calculated from the results of the least-squares fit presented in Table II. The circles represent difference frequency laser observations and the squares diode laser observations.

from the upper state level constants by forming a linear combination of parameters such that a parameter representing the location of the upper state level is replaced by a parameter corresponding to the average frequency of all the observed lines ending on the upper state level. The normal matrix then becomes block diagonal with one block for the ground-state constants and a series of 1×1 blocks for the average frequencies. In this fit, 40 microwave lines, 37 FIR LMR lines, and 900 ν_1 infrared lines were used involving 332 upper state levels. (There appear to be more ν_1 lines used than were given as measured and assigned because unresolved spin and asymmetry doublets were each treated as two lines at half weight in the fit.) Each data point was weighted by the squared reciprocal of the estimated

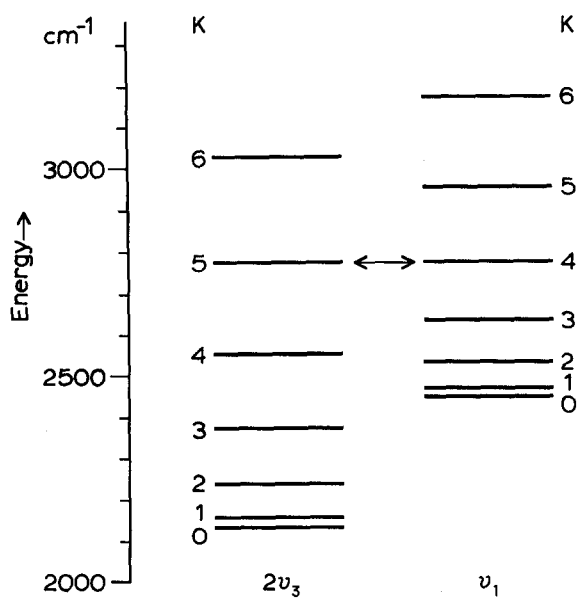

FIG. 5. Estimated locations of the hypothetical $N = 0$ energy levels for the $2\nu_3$ and ν_1 states. It is believed that the $K = 4$ level of ν_1 is being perturbed by an anharmonic Coriolis interaction with $K = 5$ of $2\nu_3$ as is indicated by the double-headed arrow. The uncertainty in the estimation of the $2\nu_3$ levels is about $\pm 40\ \text{cm}^{-1}$.

measurement uncertainty (microwave $= 1\times10^{11}$, FIR LMR $= 1\times10^{8}$, diode $= 1\times10^{6}$, difference frequency $= 1\times10^{4}$).

In the Hamiltonian used there are 23 parameters for a given vibrational state corresponding to 3 rotational constants, 5 quartic, 4 sextic, and 1 octic centrifugal distortion parameters (the 3 off diagonal in K sextic constants are omitted and only the K^8 octic term is included), 4 spin–rotation interaction constants, 5 quartic spin–rotation centrifugal distortion constants (Δ^s_{NK} is omitted), and 1 sextic spin–rotation distortion constant (Φ^s_K). Even the large number of lines fitted are insufficient to determine all of these parameters. In order to truncate the Hamiltonian to a set of determinable parameters, the diagnostic least-squares method[25] was used to identify the poorly determined parameters (Φ_N, δ^s_N, δ^s_K). This resulted in a fit using the method just described giving the ground-state rotational, centrifugal distortion, and spin–rotational parameters listed in Table II.

The weighted standard deviation of this fit is 1.1 which is what is expected from the estimated errors in the observations. However, it must be pointed out that the residuals are not distributed very smoothly. Sears[16] recognized a problem in the ground-state fitting in that in a combined fit of the microwave[15] and FIR LMR[16] transitions, several of the FIR LMR lines have large residuals. Moreover, the fit of the microwave data is poorer than the expected experimental error. (The ν_1 data is actually fitted somewhat better than the estimated experimental error.) One pair of FIR LMR lines ($N\,11 \leftarrow 10, K = 6$) have by far the largest weighted residuals and appear to have a spin–rotation splitting which is too small. However, eliminating these two lines is not sufficient to make the distribution of residuals smooth. We believe that the ground-state parameters given in Table II are the best synthesis of the information currently available.

The ground-state parameters were then fixed at the values in Table II and the excited state rotational, centrifugal distortion, and spin–rotational constants as well as the band origin were determined by fitting the infrared transition frequencies. Once again the diagnostic least-squares procedure was used to decide which parameters are determinable guiding the truncation of the Hamiltonian. In this fit $K' = 4$ lines

TABLE II. Parameters resulting from least-squares fit of the infrared, FIR LMR, and microwave data on HCO.

Parameter (cm^{-1})		(000)[a]	(000)[b]	(100)[c]
	ν_0			2434.477 90(24)
	$\mathscr{A} - (\mathscr{B} + \mathscr{C})/2$	22.882 726(11)	22.883 296 1(86)[d]	21.142 25(37)[d]
	$(\mathscr{B} + \mathscr{C})/2$	1.446 310 2(4)	1.446 309 91(28)	1.445 180 0(26)
10^2	$(\mathscr{B} - \mathscr{C})/4$	2.382 4(16)	2.382 1(11)	2.524 91(64)
10^6	Δ_N	3.952(19)	3.953(13)	4.011 3(71)
10^5	Δ_{NK}	1.520(13)	1.524 4(96)	−0.490(56)
10^2	Δ_K	3.068 91(96)	3.141 15(83)	2.696(14)
10^7	δ_N	3.911(43)	3.841(33)	4.298(48)
10^4	δ_K	1.50(16)[e]	1.47(11)	1.404(53)
10^9	Φ_{NK}		2.7(12)	f
10^7	Φ_{KN}	−4.718(87)	−4.860(98)	−9.80(21)
10^4	Φ_K		1.472(11)	1.29(14)
10^7	$L_K^{(4)}$		6.82(35)	0.2(38)
10	$\epsilon_{aa} + \epsilon_{bb} + \epsilon_{cc}$	3.814 48(40)	3.814 01(27)	3.294 2(34)
10	$2\epsilon_{aa} - \epsilon_{bb} - \epsilon_{cc}$	7.817 05(67)	7.816 06(45)	6.766 5(70)
10^3	$(\epsilon_{bb} - \epsilon_{cc})/2$	3.743 9(24)	3.746 2(18)	3.700(78)
10^3	ϵ_{ab}	6.72(8)	6.504(53)	f
10^7	Δ_N^s	2.10(33)	2.34(27)	f
10^6	Δ_{NK}^s	−3.32(73)	−1.65(53)	f
10^3	Δ_K^s	−1.637(12)	−1.603 3(75)	−1.295(17)
10^6	Φ_K^s	4.45(88)	1.56(54)	f
	σ_{weighted}[g]		1.1	0.9

[a] Reference 16.
[b] This work.
[c] This work.
[d] Uncertainties are one estimated standard deviation in last two reported digits. For the (1,0,0) level the uncertainty applies to the *difference* between (1,0,0) and (0,0,0) constants.
[e] Corrected uncertainty, personal communication, T. J. Sears.
[f] Constrained to ground-state value.
[g] The weighting is such that the expected standard deviation is 1.0.

were omitted because of the suspected perturbation previously mentioned. In the final fit, 705 transitions were used: 150 diode laser and 555 difference frequency laser measurements. Table II presents the resulting excited state constants and the band origin. Note the rather large changes in Δ_{NK} and Φ_{KN} from the ground state. Similar changes are found even if the $K' = 5$ lines are omitted, i.e., if only lines of $K' = 0, 1, 2$, and 3 are included. It is possible that some of the $K' = 3$ levels are experiencing a small perturbation.

In this two step treatment of the infrared data, the estimated standard deviations of the excited state constants are statistically all too small as they do not properly reflect the uncertainties in the ground-state constants. Rather the uncertainty listed for an excited state constant in Table II is more accurately thought of as an uncertainty in the *difference* between the ground-state and excited-state value. Of course, in addition to the statistical uncertainties, the inadequacy of the model that must be used should be kept in mind in any further use of the upper state constants reported here.

Equilibrium constants

The rotational and centrifugal distortion constants obtained here can be combined with those obtained in previous high resolution studies of the bending and CO stretch fundamentals to calculate the vibration–rotation interaction constants. These constants are listed in Table III. In Table III it is considered that the ground-state rotational constants resulting from fitting the bending and CO stretch fundamentals are somewhat different from the values given in Table II. For this reason the differences between the ground and excited state constants obtained in these studies were used rather than the absolute values of the excited state constants since these differences are believed to be better determined.

From the vibration–rotation interaction constants, the centrifugal distortion constants, and rotational g factors, equilibrium rotational constants and moments of inertia of HCO may be calculated and are listed in Table IV. The two centrifugal distortion constants needed to correct the rotational constants for centrifugal distortion effects, R_6 and τ_{abab}, were calculated from the constants listed in Table II by finding the expressions for Δ_N, Δ_{NK}, Δ_K, δ_N, and δ_K in terms

TABLE III. α constants and $\frac{1}{2}\Sigma^s \alpha_s^i$ of HCO (cm^{-1}).

s		α_s^A	α_s^B	α_s^C
1[a]		1.7422(4)[b]	−0.001 73(2)	0.003 99(2)
2[c]		0.1012(2)	0.012 53(6)	0.011 52(6)
3[d]		−2.2463(1)	−0.006 33(5)	0.006 10(7)
	$\frac{1}{2}\sum_s \alpha_s^i$	−0.2015(2)	0.002 24(4)	0.010 81(5)

[a] This work.
[b] Values in parentheses correspond to one standard deviation.
[c] Reference 2.
[d] Reference 5.

TABLE IV. Calculation of equilibrium rotational constants (cm^{-1}) and moments of inertia ($uÅ^2$) of HCO.

$\mathscr{A}$[a]	24.128 2(2)	A[b]	24.128 2	A'[c]	24.128 0	A_e[d]	24.315 3
$\mathscr{B}$	1.496 20(4)	B	1.496 06	B'	1.495 83	C_e	1.495 85
$\mathscr{C}$	1.409 47(5)	C	1.409 61	C'	1.409 95	C_e	1.410 15

Equilibrium moments of inertia

I_a^e	0.693 290
I_b^e	11.269 5
I_c^e	11.954 5
Δ_e	−0.008 4

[a] Equilibrium $\mathscr{A}$, $\mathscr{B}$, $\mathscr{C}$ from the α's of Table III and the ground-state rotational constants of Table II.

[b] Ground state $R_6 = -3.3\times10^{-8}$ cm^{-1} with the equilibrium centrifugal distortion constants assumed equal to the ground state.

[c] Ground state $\tau_{abab} = -4.5\times10^{-4}$ cm^{-1} and equilibrium assumed equal to ground state.

[d] Rotational g values calculated from the formula $g_{ii} = -|\epsilon_{ii}|/\zeta$ (Ref. 26) with ζ assumed equal to 50 cm^{-1} (Ref. 2).

of the four independent planar centrifugal distortion constants τ_{aaaa}, τ_{bbbb}, τ_{aabb}, and τ_{abab} and then least-squares fitting the five Δ's (weighted using the reciprocal of their covariance matrix) with the four τ's. The resulting R_6 and τ_{abab} are given in the footnote to Table IV. The rotational g factors needed for the electron slippage correction may be estimated for the spin–rotation interaction constants using the equation[26] $g_{ii} = -|\epsilon_{ii}|/\zeta$, with[6] $\zeta = 50$ cm^{-1}. The inadequacy of this method for finding approximate values of the g_{ii}'s is probably the reason that the equilibrium inertial defect is so large. In order to determine the equilibrium structure of HCO, a similar treatment of DCO is required. Such a treatment is not possible at this time because the bending fundamental of DCO has not been observed under high resolution.

Transition dipole orientation

The orientation of the transition dipole moment for ν_1 with respect to the principal axes was obtained by measuring the relative intensities of parallel and perpendicular rotational components. The intensities of 90 pairs of difference frequency laser absorption lines with common ground-state rotational levels were compared. Although there is considerable scatter in these relative intensity measurements, the scatter in the angle which the transition dipole moment makes with the axes is relatively small because the arc tangent of the square root of the intensity ratio is involved. The result is that the transition dipole moment makes an angle of $63 \pm 6°$ with the b axis. Using the equilibrium structure estimated by Hirota,[1] one can calculate the orientation of the CH bond of 41° with the b axis. Thus the transition dipole makes an angle of 22° (or with the less reasonable choice of signs 76°) with the CH bond. This is illustrated in Fig. 7. As the H atom moves away from the C atom, there must be significant motion of the electron density along the CO bond.

DISCUSSION

The CH stretching frequency determined here, 2434.48 cm^{-1}, is well within the range of 2432 ± 20 determined by

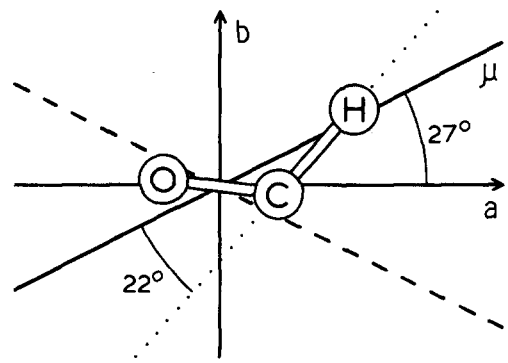

FIG. 7. Orientation of the transition dipole moment for ν_1 in the molecule. The line marked μ is the most reasonable orientation; the dashed line is the orientation which results from the other choice of the relative signs of the a and b components of the transition dipole.

LIF[14] and of 2440 ± 20 by photoelectron spectroscopy.[21] The *ab initio* value of 2448 cm^{-1} is too high by only 0.6%.[27] The much higher frequency observed in an Ar matrix[13] implies a matrix shift of 48 cm^{-1} to the blue. Jacox has suggested that this anomalously large stiffening of the CH stretch is a consequence of the unusually low dissociation energy, low vibrational frequency, and large anharmonicity.[28]

Because the CH bond of HCO is unusually weak and anharmonic, there is considerable interest in mapping out the complete potential energy surface of the molecule. A high quality *ab initio* surface has been developed.[27] Hirota[1] has determined quadratic and cubic force constants from the fundamental frequencies and high resolution vibration–rotation constants available in 1985. The improved centrifugal distortion constants for the ground state and especially the new constants for ν_1 resported here should permit a significantly improved force field to be defined. An even better determined force field should result from the investigation of combination bands especially the Fermi resonance between $2\nu_3$ and ν_1, or even better, between $\nu_1 + 2\nu_3$ and $2\nu_1$ which would directly determine the cubic force constant linear in the CH stretch and quadratic in the bend. The ν_3 band of DCO also remains to be studied at high resolution. In HCO the high resolution study of $2\nu_1$ and possibly combinations thereof with ν_3 and ν_2 should produce valuable information about the nature of the potential surface and nuclear motions on that surface near the CH dissociation threshold.

ACKNOWLEDGMENTS

The work at Rice University was supported by Robert A. Welch Foundation Grant No. C-071 and NSF Grant No. CHE-8504171. The work at the University of California was supported by Director, Office of Energy Research, Office of Basic Energy Sciences, Chemical Sciences Division of the U.S. Department of Energy under Contract No. DE-AC03-76F00098. We would like to express our appreciation to Professor John Hutchinson and the members of his research group for their generous help with and support of the computations, to Trevor Sears for his help with the energy calculation programs, and to Hrvoje Petek for his assistance with the difference frequency spectroscopy.

[1]E. Hirota, J. Mol. Struct. **146**, 237 (1986).
[2]J. W. C. Johns, A. R. W. McKellar, and M. Riggin, J. Chem. Phys. **67**, 2427 (1977).
[3]B. M. Landsberg, A. J. Merer, and T. Oka, J. Mol. Spectrosc. **67**, 459 (1977).
[4]J. M. Brown, J. Buttenshaw, A. Carrington, K. Dumper, and C. R. Parent, J. Mol. Spectrosc. **79**, 47 (1980).
[5]J. M. Brown, K. Dumper, and R. S. Lowe, J. Mol. Spectrosc. **97**, 441 (1983).
[6]R. S. Lowe and A. R. W. McKellar, J. Chem. Phys. **74**, 2686 (1981).
[7]H. Petek, D. J. Nesbitt, P. R. Ogilby, and C. B. Moore, J. Phys. Chem. **87**, 5367 (1983).
[8]A. S. Pine, J. Opt. Soc. Am. **64**, 1683 (1974); **66**, 97 (1976).
[9]S. Gerstenkorn and P. Luc, *Atlas du spectre d'absorption de la molecule d'iode* (CNRS, Paris, 1980).
[10]R. Spence and W. Wild, J. Chem. Soc. **1935**, 338.
[11]C. B. Dane, R. Bruggemann, R. F. Curl, J. V. V. Kasper, and F. K. Tittel, Appl. Opt. **26**, 95 (1987).
[12]G. Guelachvili and N. Rao, *Handbook of Infrared Standards* (Academic, Orlando, FL, 1986).
[13]D. E. Milligan and M. E. Jacox, J. Chem. Phys. **51**, 277 (1969).
[14]B. M. Stone, M. Noble, and E. K. C. Lee, Chem. Phys. Lett. **118**, 83 (1985).
[15]G. A. Blake, K. V. L. N. Sastry, and F. C. DeLucia, J. Chem. Phys. **80**, 95 (1984).
[16]T. J. Sears, Comput. Phys. Rep. **2**, 1 (1984).
[17]R. S. Timonen, E. Ratajczak, and D. Gutman, J. Phys. Chem. (in press).
[18]J. K. G. Watson, in *Vibrational Spectra and Structure, A Series of Advances*, edited by J. R. Durig (Elsevier, Amsterdam, 1977), Vol. VI.
[19]J. M. Brown and T. J. Sears, J. Mol. Spectrosc. **75**, 111 (1979).
[20]T. J. Sears, Comput. Phys. Commun. **34**, 123 (1984).
[21]K. K. Murray, T. M. Miller, D. G. Leopold, and W. C. Lineberger, J. Chem. Phys. **84**, 2520 (1986).
[22]J. M. Flaud and C. Camy-Peyret, J. Mol. Spectrosc. **51**, 142 (1974).
[23]D. L. Albritton, W. J. Harrop, A. L. Schmeltekopf, R. N. Zare, and E. L. Crow, J. Mol. Spectrosc. **46**, 67 (1973).
[24]R. F. Curl and C. B. Dane, J. Mol. Spectrosc. (in press).
[25]R. F. Curl, J. Comput. Phys. **6**, 367 (1970).
[26]C. E. Barnes, J. M. Brown, A. Carrington, J. Pinkstone, T. J. Sears, and P. J. Thistlethwaite, J. Mol. Spectrosc. **72**, 86 (1978).
[27]J. M. Bowman, J. S. Bittman, and L. B. Harding, J. Chem. Phys. **85**, 911 (1986).
[28]M. E. Jacox, Chem. Phys. Lett. **56**, 43 (1978).